A NIMA-related kinase, CNK4, regulates ciliary stability and length

Dan Meng[a] and Junmin Pan[a,b,*]
[a]MOE Key Laboratory of Protein Sciences, School of Life Sciences, Tsinghua University, Beijing 100084, China;
[b]Laboratory for Marine Biology and Biotechnology, Qingdao National Laboratory for Marine Science and Technology, Qingdao 266071, China

ABSTRACT **NIMA-related kinases (Nrks or Neks) have emerged as key regulators of ciliogenesis. In human, mutations in *Nek1* and *Nek8* cause cilia-related disorders. The ciliary functions of Nrks are mostly revealed by genetic studies; however, the underlying mechanisms are not well understood. Here we show that a *Chlamydomonas* Nrk, CNK4, regulates ciliary stability and length. CNK4 is localized to the basal body region and the flagella. The *cnk4*-null mutant exhibited long flagella, with formation of flagellar bulges. The flagella gradually became curled at the bulge formation site, leading to flagellar loss. Electron microscopy shows that the curled flagella involved curling and degeneration of axonemal microtubules. *cnk4* mutation resulted in flagellar increases of IFT trains, as well as its accumulation at the flagellar bulges. IFT speeds were not affected, however, IFT trains frequently stalled, leading to reduced IFT frequencies. These data are consistent with a model in which CNK4 regulates microtubule dynamics and IFT to control flagellar stability and length.**

Monitoring Editor
Stephen Doxsey
University of Massachusetts

Received: Oct 13, 2015
Revised: Dec 7, 2015
Accepted: Jan 4, 2016

INTRODUCTION

Eukaryotic flagella and cilia are motile and sensory organelles. Impairment of proper ciliogenesis or ciliary signaling is associated with a class of diseases and developmental disorders termed ciliopathies (Badano *et al.*, 2005; Brown and Witman, 2014). Ciliary assembly and maintenance require intraflagellar transport (IFT), which delivers ciliary precursors to the assembly site at the ciliary tip and returns turnover products to the ciliary base within the cell body (Rosenbaum and Witman, 2002; Scholey, 2003). Anterograde and retrograde transport of IFT are driven by kinesin-2 and cytoplasmic dynein 1b, respectively. IFT motors carry large protein complexes called IFT complexes, consisting of complexes A and B, that serve as cargo adaptors for ciliary components. IFT complexes appear as small particles that are bridged with each other to form so-called IFT trains (Pigino *et al.*, 2009). Defects in IFT may block or impair ciliogenesis (Pedersen and Rosenbaum, 2008).

In differentiated ciliated cells, cilia keep their structural integrity and length to perform ciliary functions (Ishikawa and Marshall, 2011). Recent evidence indicates that the ciliary length is controlled by a length-sensing system (Rosenbaum, 2003; Chan and Marshall, 2012; Cao *et al.*, 2013). The length-generated signaling is predicted affect several cellular processes, including transcription, IFT, dynamics, and stability of axonemal microtubules (Ishikawa and Marshall, 2011; Chan and Marshall, 2012). Various protein kinases play key roles in ciliary length control (Cao *et al.*, 2009; Lefebvre, 2009; Ishikawa and Marshall, 2011). The balance between the rates of axonemal assembly and disassembly mediated by IFT and protein turnover, respectively, was suggested to determine the final ciliary length (Marshall and Rosenbaum, 2001).

NIMA-related kinases (Nrks or Neks) are a group of kinases that share closer homology with NIMA than any other class of kinases and have been identified in organisms ranging from unicellular eukaryotes to multicellular organisms (O'Connell *et al.*, 2003; Fry *et al.*, 2012). Eleven genes in the human genome encode Nek1 to Nek11. In *Chlamydomonas*, 12 Nrks have been identified, including FA2 and CNK1-11 (Parker *et al.*, 2007; Lin *et al.*, 2015). Nrks play essential roles in mitotic progression, DNA repair, and microtubule dynamics. They are also involved in ciliogenesis, as demonstrated in

This article was published online ahead of print in MBoC in Press (http://www.molbiolcell.org/cgi/doi/10.1091/mbc.E15-10-0707) on January 13, 2016.

*Address correspondence to: Junmin Pan (panjunmin@tsinghua.edu.cn).

Abbreviations used: CNK, Chlamydomonas MIMA–related kinase; IFT, intraflagellar transport; NaPPi, sodium pyrophosphate; Nrks, NIMA-related kinases; WT, wild type.

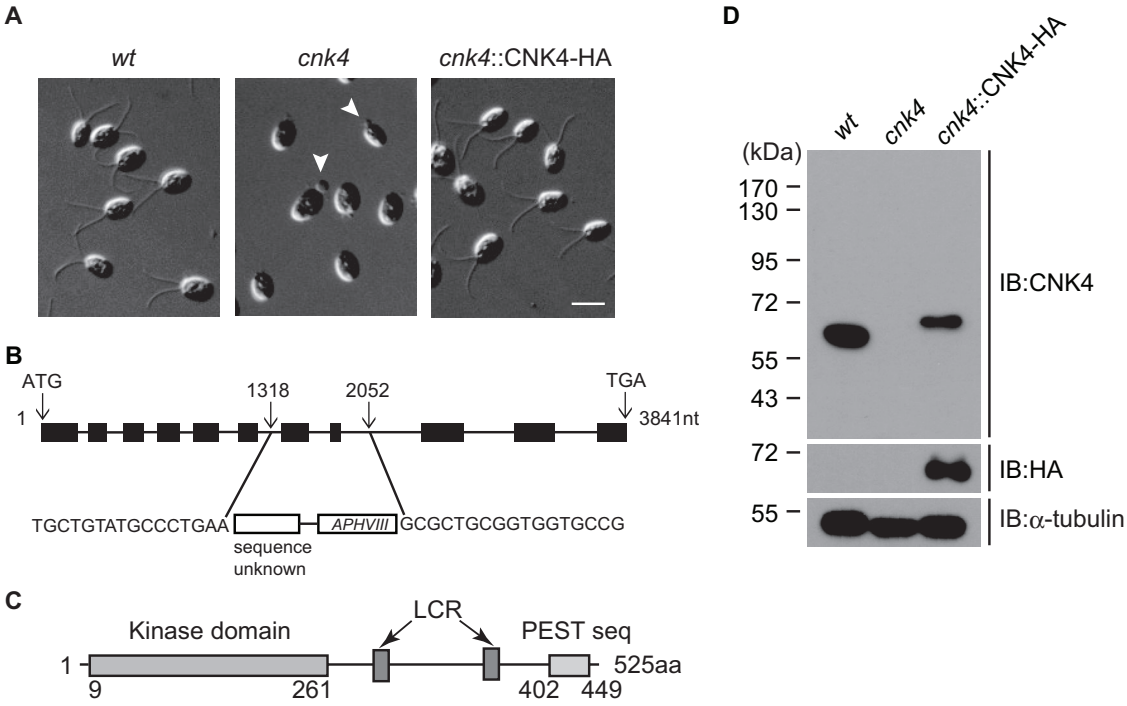

FIGURE 1: *cnk4* is defective in ciliogenesis. (A) Wild-type (*wt*), *cnk4*, and *cnk4*::CNK4-HA cells were imaged by DIC microscopy. Note that *cnk4* cells are aflagellated or have flagellar buds (arrowheads). Bar, 10 μm. (B) Schematic illustration of the *CNK4* gene, showing the replacement of exons 7 and 8 by foreign DNA fragment during random DNA insertion. The insertion site was identified by PCR and DNA sequencing. (C) The domain structure of CNK4. Numbers are amino acid positions. LCR, low-complexity region. (D) Western blot of whole-cell lysates from indicated strains with antibodies against CNK4, HA, and α-tubulin. No CNK4 was detected in the *cnk4* mutant.

Chlamydomonas, *Tetrahymena*, *Trypanosome*, mice, and humans (Fry *et al.*, 2012; Meirelles *et al.*, 2014; Kim *et al.*, 2015).

In *Chlamydomonas*, CNK2 suppresses the dynamics of axonemal microtubules to control flagellar length (Hilton *et al.*, 2013). CNK11 inhibits flagellar length only in mutants defective in flagellar substructures, although the underlying mechanism is unknown (Lin *et al.*, 2015). Human mutations in *Nek1* cause short-rib polydactyly syndrome, type Majewski, characterized by malformation of the brain, polydactyly, and kidney cyst, consistent with ciliary defects (Thiel *et al.*, 2011). Depletion of Nek1 in kat2J mouse mesenchymal fibroblasts or in cell cultures reduces the number of ciliated cells. Surprisingly, a portion of remaining cilia are long and branched (Shalom *et al.*, 2008; Wang *et al.*, 2014).

We characterized CNK4 in *Chlamydomonas*. *cnk4*-null mutation induces long flagella that are gradually destabilized, resulting in final flagellar loss.

RESULTS

A *Chlamydomonas* flagellar mutant defective in *CNK4*

We used insertional mutagenesis to identify genes required for ciliogenesis in *Chlamydomonas*. A DNA fragment harboring the paromomycin resistance gene *AphVIII* was used for transformation (Sizova *et al.*, 2001; Meng *et al.*, 2014). The mutations can be caused by random insertion and/or deletion of flanking genomic DNA (Galvan *et al.*, 2007; Jinkerson and Jonikas, 2015). Wild-type cells have two equal-length flagella of ~12 μm. One mutant has no flagella or only flagellar buds, indicating ciliogenesis defects (Figure 1A). The flanking sequence of the insert in the mutant was cloned by restriction enzyme site–directed amplification (RESDA) PCR (Gonzalez-Ballester *et al.*, 2005; Meng *et al.*, 2014) and sequenced. The disrupted gene was identified as *CNK4*, encoding a protein kinase of 525 amino acids (aa). Further analysis showed that the *CNK4* nucleotide sequence 1318–2052 was deleted and replaced by the *AphVIII* gene fragment and an unknown sequence, resulting in removal of exons 7 and 8 (Figure 1B).

CNK4 has an N-terminal kinase domain, a PEST sequence at the C-terminus, and two low-complexity regions predicted by SMART and EMBOSS websites (Figure 1C). A BLAST search of CNK4 kinase domain in the human proteome showed that CNK4 has closer sequence identity to NEK1 (Supplemental Table S1). However, CNK4 has only 525 aa, whereas NEK1 has 1258 aa, and does not have the coil-coil domain predicted in Nek1 (Fry *et al.*, 2012). Immunoblot analysis showed that *cnk4* does not express CNK4 (Figure 1D), indicating that *cnk4* is a null mutant. Transformation of *cnk4* with hemagglutinin (HA)-tagged *CNK4* restored CNK4 expression and recovered the wild-type (wt) flagellar phenotype (Figure 1, A and D). Because >20% of transformants rescued the mutant phenotype from at least three independent transformations, this rescue was caused by incorporation of the transgene and not by disruption of some other genes. Therefore *CNK4* is the causal gene in the *cnk4* mutant.

CNK4 is a flagellar protein

Nrks with ciliary functions are usually located at the ciliary structures. *Chlamydomonas* FA2 and CNK2 are localized to proximal flagella and along the axoneme, respectively (Mahjoub *et al.*, 2004; Bradley and Quarmby, 2005). Both Nek1 and Nek2 localize to the basal body, whereas Nek8 is located at the proximal cilium (Mahjoub *et al.*, 2005; Shalom *et al.*, 2008; Sohara *et al.*, 2008; Spalluto *et al.*, 2012; Kim *et al.*, 2015). To determine the cellular

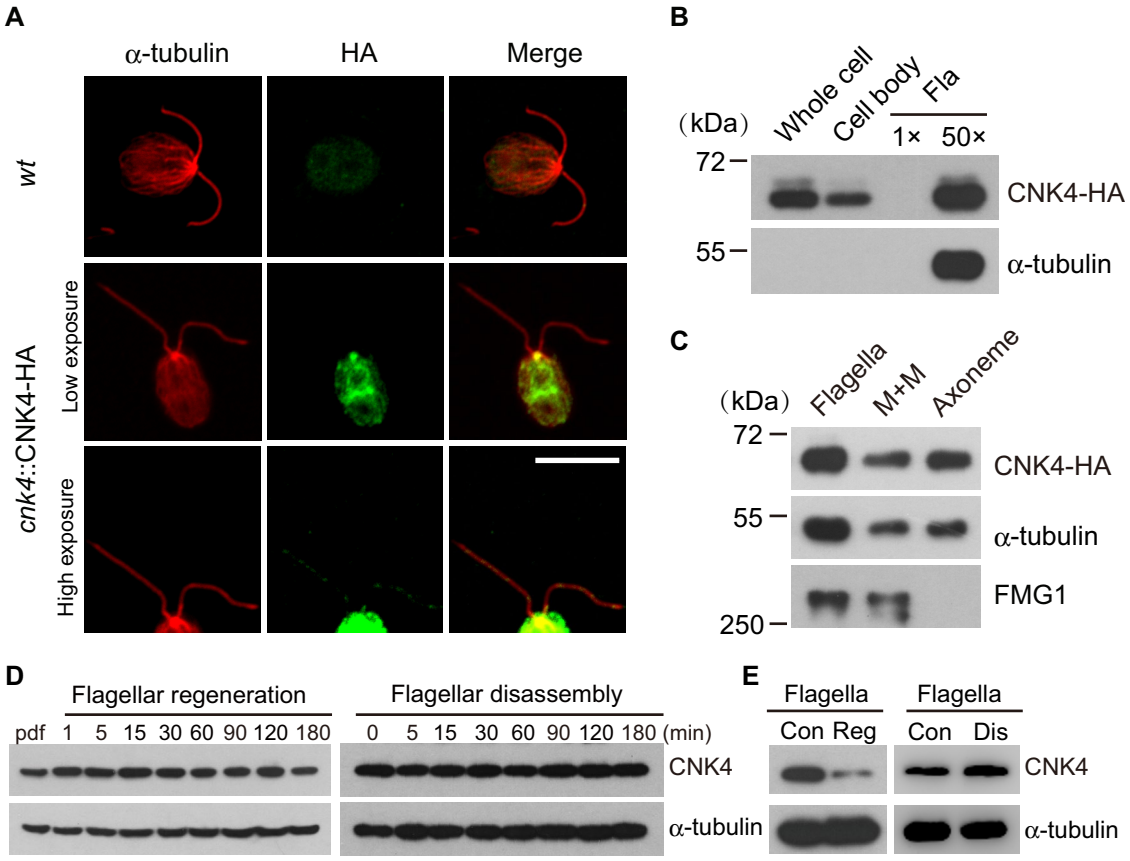

FIGURE 2: CNK4 is a flagellar protein. (A) CNK4 is localized to flagella and basal body. *wt* and *cnk4*::CNK4-HA cells were immunostained with anti-HA and anti–α-tubulin antibodies, respectively. High-exposure images show the flagellar location of CNK4. Bar, 10 μm. (B) *cnk4*::CNK4-HA cells were fractionated into cell body and flagella, followed by immunoblotting. Here 1×Fla (flagella) represents equal proportion of flagella to the cell body. (C) Isolated flagella of *cnk4*::CNK-HA cells were fractionated into membrane matrix (M+M) and axonemal fractions, followed by immunoblotting. FMG1 is a membrane protein. (D) *wt* cells were allowed to regenerate flagella after deflagellation (left) or treated with sodium pyrophosphate (NaPPi) to induce flagellar disassembly (right), followed by immunoblotting. (E) Flagella were isolated during flagellar regeneration after deflagellation or flagellar disassembly induced by NaPPi, followed by immunoblotting. Con, steady-state flagella; Dis, disassembling flagella; Reg, regenerating flagella.

location of CNK4, we immunostained the rescued strain expressing CNK4-HA with antibodies against HA and α-tubulin with *wt* cells as control (Figure 2A). CNK4 is localized to several regions within the cell body, which includes prominent staining at the basal body. High exposure of the images also revealed punctate staining of CNK4 in the flagella. The presence of CNK4 in the flagella was further verified by immunoblotting of isolated flagella (Figure 2B). To pinpoint the location of CNK4 in the flagellar compartment, we further fractionated isolated flagella into membrane matrix (M+M) and axonemal fractions, followed by immunoblotting. The membrane protein FMG1 (Bloodgood and Salomonsky, 1994) and α-tubulin were used as controls. CNK4 is localized to both membrane matrix and axonemal fractions (Figure 2C).

The cellular location of CNK4 and the mutant flagellar phenotype implicate CNK4 in ciliogenesis. Next we examined CNK4 protein expression during flagellar assembly or disassembly. Cells were allowed to undergo flagellar assembly after deflagellation or treated with sodium pyrophosphate to induce flagellar disassembly. The expression level of CNK4 during both processes showed no apparent changes, as examined by immunoblotting of whole-cell extracts (Figure 2D). Nor did we find molecular shift of CNK4, which is usually associated with protein phosphorylation. Examination of isolated flagella by immunoblotting showed that CNK4 decreased during flagellar regeneration and slightly increased during flagellar disassembly, indicating that CNK4 is likely involved in flagellar assembly and disassembly (Figure 2E).

cnk4 fails to maintain flagella by forming bulges and flagellar balloons

Under light/dark synchronization growth conditions, *Chlamydomonas* undergoes several rounds of continuous division within the mother cell wall in the dark period (Cross and Umen, 2015). The daughter cells with fully assembled flagella are then released. Cells that are unable to form flagella fail to be released from the cell wall, leading to formation of palmelloids or cysts (Kubo *et al.*, 2009; Wood *et al.*, 2013). Most *cnk4* cells were aflagellate but did not form palmelloids (Figure 1A). Thus we examined whether *cnk4* could form flagella after cell division (Figure 3A). *wt* cells divided soon after entering the dark period, and the flagellated daughter cells were completely released after 5 h. In contrast, *cnk4* cells had an early onset of cell division, and the daughter cells were only released upon onset of the light period. This phenotype is also caused by *CNK4* mutation, as *CNK4*-rescued strains did not show this phenotype. Treatment of *cnk4* cells with light at 4 h in the dark period

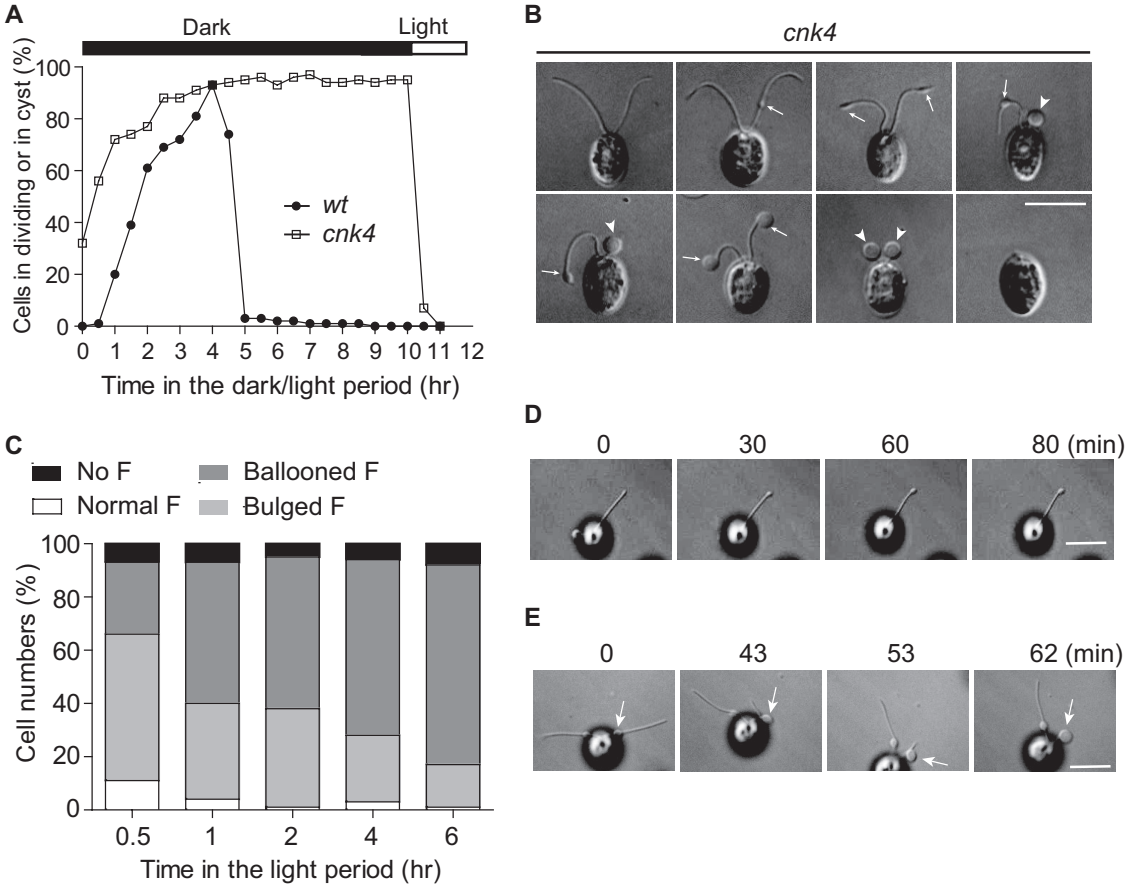

FIGURE 3: *cnk4* loses flagellar maintenance by forming flagellar bulges and balloons. (A) Cells were synchronized by using light/dark cycles under 5% CO_2. *cnk4* cells exhibited early onset of cell division, and the daughter cells were released upon lighting, whereas *wt* cells released daughter cells after completion of cell division. (B) DIC images of *cnk4* cells show distinct flagellar phenotypes. The flagellar bulges and balloons are marked as arrows and arrowheads, respectively. Bar, 10 μm. (C) Quantification of different types of flagella after cells were released in the light period. F, flagella. (D, E) Movie stills showing flagellar bulge formation (D) and flagellar curling at the bulge formation site (E). Arrows mark the bulges. Note that the distal flagellum to the bulge is retracted into the bulge. Bars, 10 μm.

induced cell release, indicating that these cells did not require longer for completion of cell division but instead that cell release requires light.

cnk4 cells released from the mother cell wall were indeed flagellated. However, these cells had striking flagellar phenotypes (Figure 3B). Instead of having two normal flagella, some cells were aflagellate or had ballooned flagella, whereas others exhibited bulges along the axoneme or at the flagellar tips. Because most *cnk4* cells were aflagellate in the late light period, these different shapes of flagella might represent different stages of flagella en route to flagellar loss. We then followed flagellar changes after cells were released from the mother cell wall. Indeed, bulged or partially curled flagella became completely curled, forming flagellar balloons as time progressed (Figure 3C).

The bulges were formed randomly along the flagellar length, and their formation was uncoordinated in the two flagella (Figure 3B). Bulge formation is likely spontaneous after flagella are assembled. Live imaging captured the formation of bulges at the flagellar tip, which took ~30 min to be clearly visible and continued to enlarge (Figure 3D and Supplemental Video S1). Of interest, we also observed that the bulge formed in the middle of flagella could migrate toward the flagellar tip (Supplemental Video S2). Large flagellar bulges and flagellar balloons were likely formed by retraction of the flagellar axoneme into the bulge formation site (Figure 3E and Supplemental Video S3). Thus the flagella gradually form bulges, which induce flagellar curling or retraction and lead to formation of ballooned flagella, which are eventually detached from the cell body.

cnk4 loses flagellar length control

cnk4 cells exhibit flagella with bulges or flagellar balloons. Surprisingly, we also observed extremely long flagella (Figure 4A). These long flagella were also associated with bulges formed randomly along the flagellar length. Next we monitored changes of flagellar length after cell release from the mother cell wall. Cells that did not form flagella or had ballooned flagella were excluded for measurement. The average flagellar length increased over time (Figure 4B). However, some cells grew extremely long flagella, >20 μm, whereas the flagellar length of *wt* cells rarely exceeds 15 μm (Berman *et al.*, 2003). Approximately 17% of flagella at 4 h after cell release are >15 μm in length. These data indicate that *cnk4* loses not only flagellar maintenance but also flagellar length control. Next we examined flagellar regeneration. Consistent with previous work *wt* cells showed rapid flagellar growth, followed by decreased rate of assembly toward steady-state length (Figure 4C; Rosenbaum *et al.*, 1969). In contrast, although *cnk4* was able to assemble flagella after

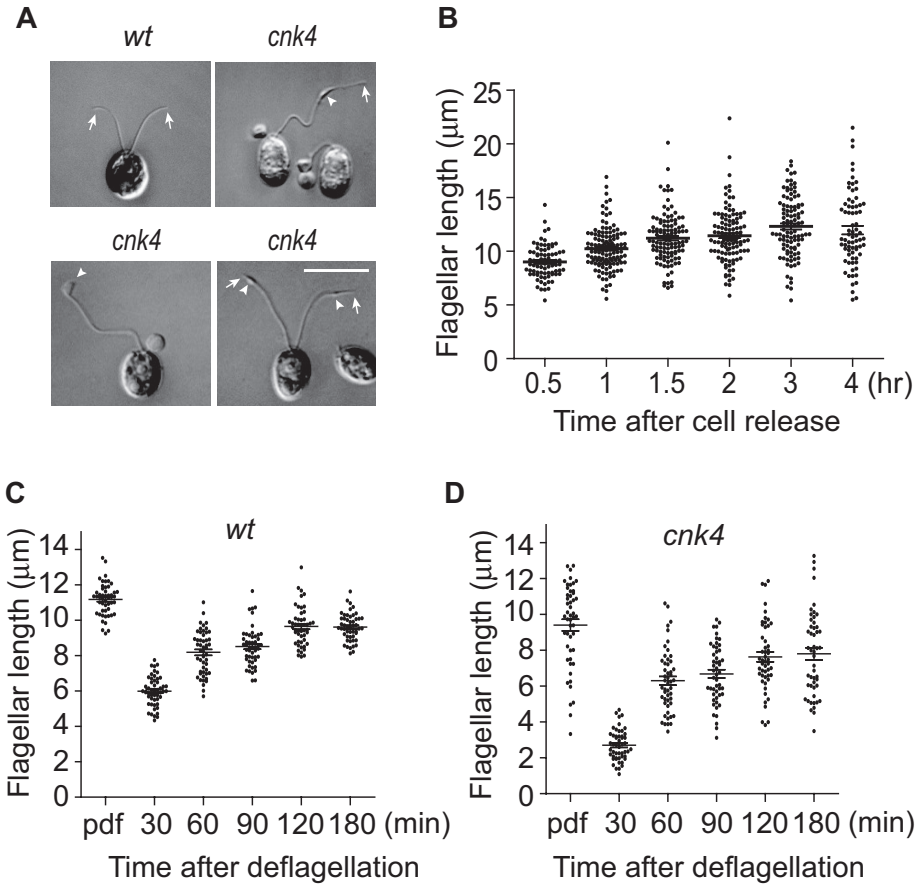

FIGURE 4: *cnk4* loses flagellar length control. (A) DIC images of *wt* and *cnk4* cells. *cnk4* cells form extremely long flagella with bulge formation (arrowheads). Arrows mark the flagellar tips. Bar, 10 μm. (B) Flagellar length increase after cells are released from the mother cell wall of *cnk4* cells. Cells were fixed at different times after cell release in the light period and imaged by DIC microscopy, followed by flagellar length measurement. Normal-looking flagella and flagella with bulges but not ballooned flagella were analyzed. (C, D) Flagellar regeneration of *wt* (C) and *cnk4* (D) cells. Cells at 1 h in the light were deflagellated by pH shock to allow flagellar regeneration, followed by flagellar length measurement. Ballooned flagella were excluded from measurement. Note that *cnk4* has a reduced rate of assembly before 30 min after deflagellation.

deflagellation, the initial flagellar assembly rate was reduced (Figure 4D). These data demonstrate that flagellar assembly in *cnk4* is dysregulated.

Accumulation of amorphous materials at flagellar bulges and destabilization of the flagellar axoneme

The formation of flagellar bulges is an early event leading to loss of flagellar maintenance. Electron microscopy revealed that *cnk4* flagellar substructures, including outer doublet microtubules, central pair apparatus, dynein arms, and radial spokes, appeared normal (Figure 5A). However, the flagellar bulges contained amorphous materials accumulated between the flagellar membrane and the outer doublet microtubules. The axonemes of the ballooned flagella were curled within the flagellar membrane, and some of the outer doublet microtubules were disorganized or degenerated (Figure 5B).

Accumulation of IFT proteins along the flagella, particularly at the bulges in *cnk4* flagella

Defects in IFT regulation or IFT components are associated with ciliary length control and accumulation of materials within the flagellum (Pedersen and Rosenbaum, 2008). Temperature-sensitive mutants *fla15* and *fla17*, which are defective in IFT144 and IFT139, respectively, form flagellar bulges randomly along the length of the flagellum (Piperno *et al.*, 1998; Iomini *et al.*, 2009). Null mutation of *MAK* induces long cilia with accumulation of IFT particles (Omori *et al.*, 2010). Therefore we examined whether *cnk4* mutation affects IFT. Examination of isolated flagella of *cnk4* revealed increases of IFT-A component IFT139, IFT-B component IFT81, anterograde IFT motor subunits FLA10 and FLA8, and retrograde motor subunit D1bLIC (Figure 6A). Because the overall protein level of IFT in whole cells of *cnk4* did not change (Supplemental Figure S1), these results indicate that *cnk4* mutation results in increased IFT proteins in the flagellum.

Next we investigated where the IFT proteins were increased in the flagella. We used antibodies against representative IFT proteins IFT139, IFT172, and FLA8 for immunostaining. In *wt* cells, IFT proteins showed prominent staining at the basal body, with faint staining along the length of flagella, which is consistent with previous work (Figure 6, B–D; Cole *et al.*, 1998). In contrast, *cnk4* flagella accumulated more IFT proteins along the length of flagella. In particular, IFT proteins heavily accumulated in the bulge region, (Figure 6B, arrow). In some bulges, IFT proteins were associated with a bulged flagellar membrane (Figure 6, C and D), indicating that IFT trains likely fall off the axonemal microtubules.

cnk4 is defective in IFT frequency, with frequent stalling of IFT

To gain further insight into the effect of *cnk4* mutation on IFT regulation, we used total internal reflection fluorescence (TIRF) microscopy to observe IFT. *IFT46-YFP* was expressed in *cnk4* cells (Figure 7A). An *ift46* mutant strain rescued by expression of *IFT46-YFP* was used as a control. In control cells, IFT trains moved smoothly in both anterograde and retrograde directions (Figure 7Ba and Supplemental Video S4). In contrast, in *cnk4* cells, IFT frequently stalled in both anterograde and retrograde directions (Figure 7Bb and Supplemental Video S5). At the bulged flagellar tip, some IFT trains underwent proper turnaround, whereas others were trapped, and trapped IFT trains might spontaneously initiate retrograde movement (Figure 7Bc and Supplemental Video S6). At the bulges formed in the middle of the flagellum, whereas some IFT trains passed the bulges freely, others were trapped (Figure 7Bd and Supplemental Video S7).

Using apparently normal flagella of *cnk4* cells, we analyzed IFT speed and frequency. The anterograde and retrograde speeds of IFT of *cnk4* cells were similar to those of controls (Figure 7C). The velocities of anterograde IFT for control and *cnk4* flagella were 1.87 ± 0.06 (64 tracks) and 1.88 ± 0.09 μm/s (202 tracks), respectively, and those of retrograde IFT were 2.46 ± 0.08 (72 tracks) and 2.48 ± 0.13 μm/s (100 tracks), respectively. As expected, anterograde and retrograde IFT frequencies were significantly reduced

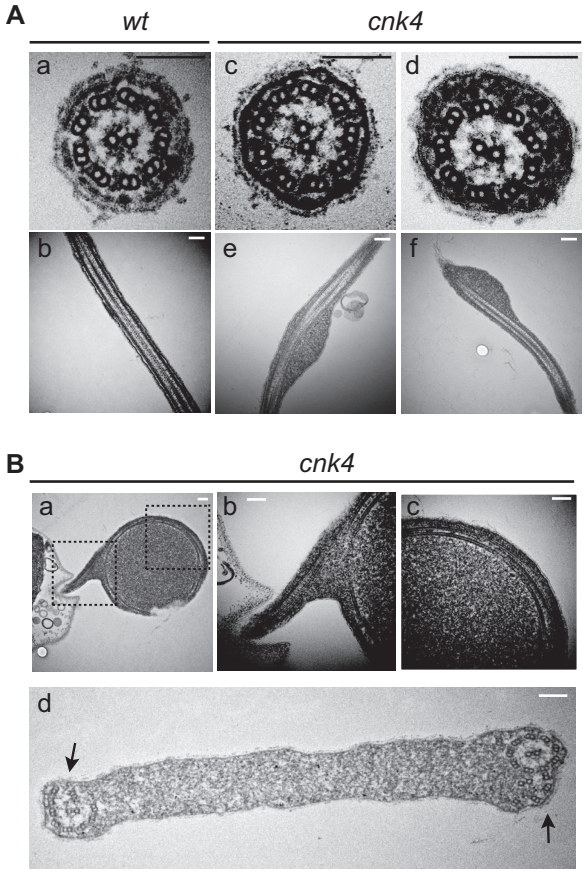

FIGURE 5: Electron microscopic analysis of *cnk4* flagella. (A) Cross- and longitudinal sections of *wt* (a, b) and *cnk4* (c–f) flagella. Note that *cnk4* flagella accumulate amorphous materials between the membrane and the axoneme (d–f), whereas its substructures appear normal (d). Bars, 150 nm. (B) Flagellar balloon cross-sectioned to show curled axoneme (a–d) and degenerated axonemal microtubules (d, arrows). Dashed box images in (a) are enlarged and shown in (b) and (c), respectively. Bars, 150 nm.

compared with those of the control, which is consistent with frequent stalling or derailing of IFT trains (Figure 7D). The anterograde frequencies for control and *cnk4* flagella were 1.21 ± 0.24 (10 flagella) and 0.86 ± 0.25 trains/s (64 flagella), respectively, and those for retrograde IFT were 0.91 ± 0.15 (10 flagella) and 0.72 ± 0.27 trains/s (65 flagella), respectively. The retrograde frequency reported here for the wild-type strain is less than that reported by using differential interference contrast (DIC) microscopy. For example, Dentler (2005) reported 1.3–1.5 trains/s. This might reflect different experimental conditions and the methods used.

DISCUSSION

We identified CNK4, an Nrk in *Chlamydomonas*, as a key regulator of ciliogenesis. *cnk4*-null mutation induces formation of long flagella with axonemal instability, leading to eventual flagellar loss, indicating that CNK4 plays an important role in ciliary length and stability.

Nrks have been increasingly recognized as critical regulators of cilia (Fry *et al.*, 2012). Four Nrks in mammalian cells have been implicated in ciliary function. Depletion of Nek1 results in reduced ciliation, as well as long and branched cilia (Shalom *et al.*, 2008; Wang *et al.*, 2014). Nek2 suppresses ciliogenesis at G2/M to ensure ciliary disassembly (Kim *et al.*, 2015). Down-regulation of *Nek4* leads to a decrease in ciliary assembly (Coene *et al.*, 2011). *nek8* missense mutation in jck mice leads to long cilia (Smith *et al.*, 2006; Sohara *et al.*, 2008). However, complete depletion of *Nek8* does not affect ciliogenesis (Manning *et al.*, 2013), indicating that the *nek8* missense mutation is likely a gain-of-function mutation. In *Chlamydomonas*, FA2 is required for flagellar autonomy, whereas CNK2 suppresses axonemal microtubule dynamics to control ciliary length (Finst *et al.*, 1998; Hilton *et al.*, 2013). CNK11 regulates flagellar length only in mutants defective in flagellar substructures (Lin *et al.*, 2015). In *Tetrahymena*, overexpression of Nrks induces ciliary shortening (Wloga *et al.*, 2006), whereas overexpression of NRKC in *Trypanosome* inhibits ciliary formation (Pradel *et al.*, 2006). These data demonstrate that Nrks are involved in different aspects of ciliary regulation, although the molecular mechanisms are mostly unknown.

Ciliary length control by CNK4

In steady-state or differentiated cells, ciliary length is kept at a constant length, which is required for optimal signaling capacity or proper motility of cilia (Ishikawa and Marshall, 2011). How ciliary length is controlled is not completely understood. The initial discovery of a long flagellar mutant *lf4* that is defective in a mitogen-activated protein (MAP) kinase suggested the possible existence of a length-sensing system (Berman *et al.*, 2003; Rosenbaum, 2003). Subsequent studies validated this notion. *Chlamydomonas* Aurora-like kinase and FLA8/KIF3B change their phosphorylation states in response to alteration of flagellar length (Luo *et al.*, 2011; Cao *et al.*, 2013; Liang *et al.*, 2014). In addition, flagellar length is associated with inverse scaling of IFT train size, and accumulation of IFT trains at the basal body is also dependent on length (Engel *et al.*, 2009; Ludington *et al.*, 2013). Ciliary length sensing is expected to trigger a signaling cascade to balance the assembly and disassembly of axonemal microtubules to achieve final ciliary length (Marshall and Rosenbaum, 2001). Multiple kinases are implicated in ciliary length control, which include LF2, LF4, LF5, GSK3, and CNK2 in *Chlamydomonas* (Berman *et al.*, 2003; Wilson and Lefebvre, 2004; Tam *et al.*, 2007, 2013; Hilton *et al.*, 2013) and intestinal cell kinase (ICK), male germ cell–associated kinase (MAK), Nek1, and Nek8 in mammalian cells (Smith *et al.*, 2006; Sohara *et al.*, 2008; Omori *et al.*, 2010; Yang *et al.*, 2013; Chaya *et al.*, 2014; Moon *et al.*, 2014). The molecular mechanisms of these kinases underlying ciliary length regulation are largely unknown. Signaling mediated by protein phosphorylation should influence processes involved in axonemal assembly such as IFT and microtubule dynamics to control ciliary length.

Alteration of IFT is expected to tilt the balance between assembly and disassembly, leading to changes of ciliary length. Temperature-sensitive mutant *fla10*, which is defective in IFT motor KIF3A/FLA10, shortens its flagella at restrictive temperature (Lux and Dutcher, 1991; Walther *et al.*, 1994; Kozminski *et al.*, 1995). Long flagellar mutant *lf4* appears to increase IFT particles at the flagellar tip (Berman *et al.*, 2003). In mammalian cells, depletion of protein kinase ICK or MAK induces formation of long cilia with accumulation of IFT proteins (Omori *et al.*, 2010; Yang *et al.*, 2013; Chaya *et al.*, 2014). The increase of IFT trains in *cnk4* flagella might function similarly to promote ciliary length.

Modulation of microtubule dynamics controls the incorporation and turnover of tubulins of axonemal microtubules at the ciliary tip. Microtubule depolymerases CrKinesin13 and KIF19A are implicated in ciliary length control (Niwa *et al.*, 2012; Wang *et al.*, 2013). Reducing polyglutamylation of axonemal microtubules increases ciliary length (Kubo *et al.*, 2015). CNK2 suppresses microtubule dynamics, and its mutation induces flagellar elongation of *lf4* (Hilton *et al.*, 2013). Given that *cnk4* mutation induces axonemal instability, CNK4

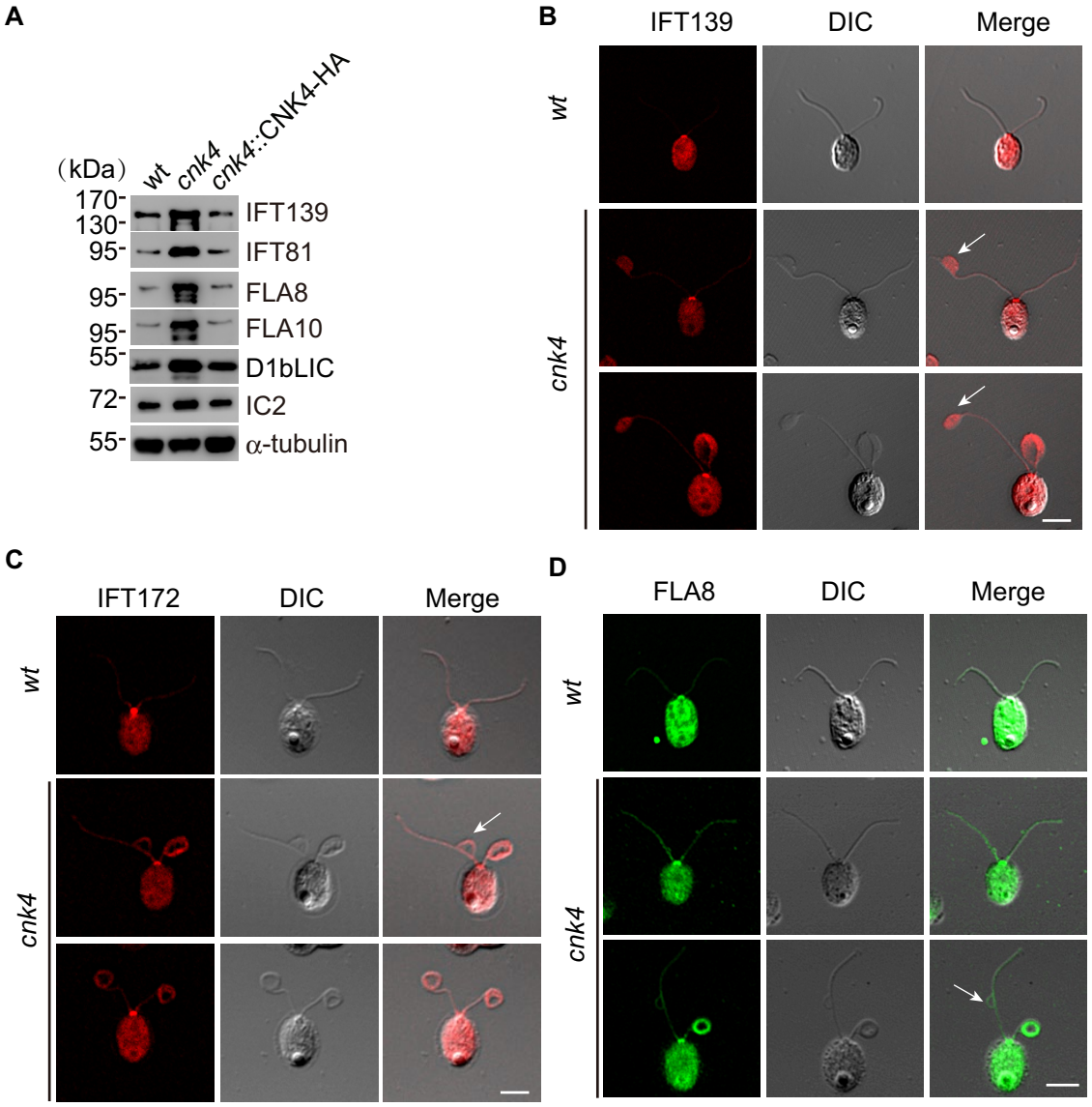

FIGURE 6: Increase of IFT proteins in the *cnk4* flagella. (A) Isolated flagella from *wt*, *cnk4*, and *cnk4*::CNK4-HA were analyzed by immunoblotting with antibodies against IFT proteins (IFT139, IFT-A; IFT81, IFT-B) and IFT motor subunits (FLA8, FLA10, and D1bLIC). IC2 and α-tubulin were used as controls. (B–D) *wt* and *cnk4* cells were immunostained with antibodies against IFT139 (B), IFT172 (C), and FLA8 (D) antibodies. *cnk4* flagella exhibit an overall increase of IFT proteins along the flagellar length compared with *wt* flagella. Flagellar bulges (arrows) are filled with IFT139, and IFT172 and FLA8 attach to the flagellar membrane. Bars, 10 μm.

might also act on microtubule dynamics to regulate ciliary length. Future identification of the targets of CNK4 will pinpoint the mechanism of CNK4 in ciliary length control.

IFT control by CNK4

IFT is under tight control. In *Chlamydomonas*, CDPK1 controls IFT ciliary entry and turnaround at the ciliary tip by regulating the phosphorylation states of the anterograde motor subunit FLA8/KIF3B (Liang *et al.*, 2014). ICK phosphorylates KIF3A, and loss of ICK leads to accumulation of IFT proteins at the tip of primary cilia (Chaya *et al.*, 2014; Moon *et al.*, 2014). Accumulation of IFT proteins in the middle of cilia is also observed in the null mutant of *MAK*, although the mechanism is unknown (Omori *et al.*, 2010). Loss of DFY-5, a MAP kinase in *C. elegans*, prevents undocking of kinesin-II at the distal end of the middle cilia segment (Burghoorn *et al.*, 2007).

cnk4 mutation leads to overall increase of IFT trains in the flagellum. We found that the frequency of IFT rather than IFT speed is affected by *cnk4* mutation. Frequent stalling of IFT is consistent with an overall increase of IFT proteins, although we could not exclude the possibility that CNK4 also regulates the IFT injection rate to bring about an increase of IFT particles (Ludington *et al.*, 2013). Frequent IFT stalling might be due to dysregulation of IFT motors, IFT particles, axonemal microtubules, and the connection between IFT trains with the ciliary membrane. We observed that IFT trains that are detached from the axonemal microtubules still associate with the flagellar membrane, indicating that this linkage is not affected. The anterograde and retrograde motors have divergent sequences. Given that IFT stalling occurs in both directions, IFT motors might not be directly affected by CNK4. The fact that both IFT-A and IFT-B components accumulate in *cnk4*-mutant flagella suggests that the

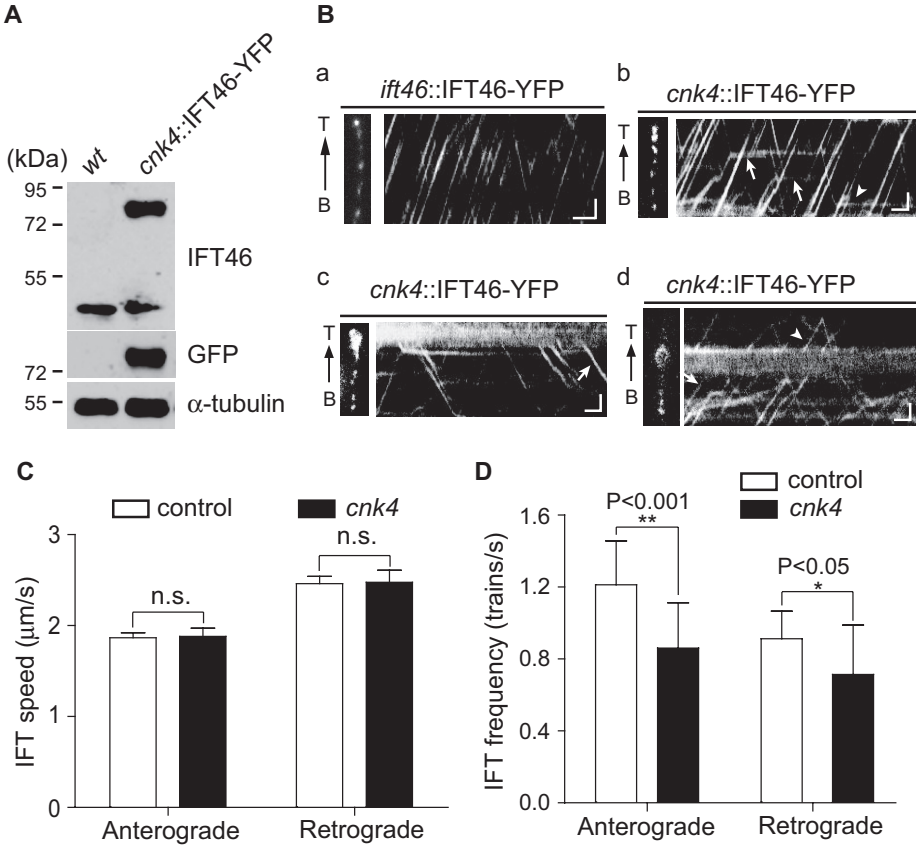

FIGURE 7: *cnk4* flagella exhibit normal IFT speed but reduced IFT frequency, with frequent IFT stalling. (A) Expression of yellow fluorescent protein (YFP)–tagged IFT46 in *cnk4*. Cells were analyzed by immunoblotting with antibodies against IFT46, GFP, and α-tubulin. (B) Kymographs of IFT46-YFP in the flagella of *ift46*::IFT46-YFP (a) and *cnk4*::IFT46-YFP (b–d) cells. Left, images of recorded flagella. (b) Kymograph from apparently normal flagellum. The arrows and arrowhead indicate stalled IFT in anterograde and retrograde directions, respectively. (c) Kymograph highlighting IFT turnaround at the bulged flagellar tip. Arrow, spontaneously initiated retrograde IFT. (d) Kymograph showing IFT at the flagellar bulge in the middle of the flagellum. Arrow, trapped IFT; arrowhead, IFT passing though the bulge. B, flagellar base; T, flagellar tip. Bars, 1 μm and 1 s. (C) The velocities of anterograde and retrograde IFT are not affected by *cnk4* mutation. n.s., not significant ($p > 0.05$). (D) IFT frequencies of both directions in *cnk4* flagella are reduced compared with those of wild-type flagella.

target of CNK4 is not individual components of IFT particles. Gene mutations of IFT-B components either block ciliary assembly or lead to formation of short flagella, whereas IFT particles rarely accumulate (Pazour *et al.*, 2000; Brazelton *et al.*, 2001; Hou *et al.*, 2007). In contrast, defects in IFT-A components result only in IFT-B accumulation (Piperno *et al.*, 1998; Iomini *et al.*, 2009). One possibility is that CNK4 affects axonemal microtubules to affect IFT. Posttranslational modifications of microtubules are implicated in regulation of motor velocity, processivity and microtubule stability (Gaertig and Wloga, 2008; Schneider *et al.*, 2008; Konno *et al.*, 2012; Sirajuddin *et al.*, 2014).

CNK4, ciliary curling, and axonemal instability

cnk4 cells form flagellar bulges, and the flagella gradually become curled at the bulge formation site, leading to eventual flagellar loss. How bulge formation leads to flagellar curling is not clear. *Chlamydomonas fla15* and *fla17* mutants form flagellar bulges due to accumulation of IFT proteins but their flagella do not curl (Piperno *et al.*, 1998; Iomini *et al.*, 2009). Thus simple accumulation of IFT proteins may not cause flagellar curling. The curling of the flagellar axoneme might involve both instability of the axoneme and loss of control of axonemal dyneins that control axonemal microtubule sliding (Witman, 1992).

MATERIALS AND METHODS

Strains and culture conditions

Chlamydomonas reinhardtii strain *21gr* (mt+; CC-1690) is available from the *Chlamydomonas* Resource Center (University of Minnesota, St. Paul, MN). *ift46*::IFT46-YFP was kindly provided by Kaiyao Huang (Institute of Hydrobiology, Chinese Academy of Sciences, Wuhan, China). Cells were cultured on 1.5% agar plates or in liquid M medium at 23°C with aeration under a 14:10-h light/dark cycle. In experiments involving cell cycle progression, cells were synchronized in 14:10-h light/dark cycles with aeration of 5% CO_2 in a Light Incubator (Percival AL-36, Percival, Perry, IA; Hu *et al.*, 2015).

Insertional mutagenesis, gene cloning, and transformation

Insertional mutants were generated by transformation with electroporation of *AphVIII* fragments (Sizova *et al.*, 2001; Liang and Pan, 2013). The genomic sequences flanking the *AphVIII* insertion site were identified by RESDA PCR and sequencing (Gonzalez-Ballester *et al.*, 2005; Meng *et al.*, 2014). To make a construct for expressing CNK4-HA in *cnk4*, the *CNK4* gene with an ~1.2-kb fragment upstream of the start codon was cloned by PCR, and a 3×HA tag sequence followed by a Rubisco terminator was cloned from plasmid pKL-3xHA (kindly provided by Karl F. Lechtreck, University of Georgia, Athens, GA; Lechtreck *et al.*, 2009). The resulting construct was cloned into a modified vector pHyg3 harboring a hygromycin B resistance gene (Berthold *et al.*, 2002). The final construct was linearized with AhdI-HF and transformed into the *cnk4* mutant using electroporation.

Cell fractionation, flagellar regeneration, flagellar shortening, flagellar length measurement, and DIC cell images

Cells were deflagellated by pH shock, followed by isolation of cell bodies and flagella or allowed for flagellar regeneration. Flagellar shortening was induced by adding 20 mM sodium pyrophosphate. Flagellar fractionation was carried out by adding 0.5% NP-40, followed by centrifugation. Cells for flagellar length measurement or examination of flagellar phenotypes were fixed by 1% glutaraldehyde and imaged by a Zeiss DIC microscope (Zeiss, Shanghai, China). The detailed procedures are essentially as described previously (Meng *et al.*, 2014).

Primary antibodies

We used the following primary antibodies: rat monoclonal anti-HA (1:50 for immunofluorescence [IF] and 1:1000 for immunoblotting [IB]; clone 3F10; Roche); mouse monoclonal anti–α-tubulin

(1:200 for IF and 1:2500 or 1:10,000 for IB; Sigma-Aldrich, Shanghai, China); mouse monoclonal anti-IC2 (1:20,000 for IB; Sigma-Aldrich); mouse monoclonal anti–green fluorescent protein (GFP; 1:2000 for IB; Abmart, Shanghai, China); mouse monoclonal anti-IFT139 (1:50 for IF and 1:10,000 for IB); mouse monoclonal anti-IFT172 (1:50 for IF); mouse monoclonal anti-IFT81 (1:1000 for IB); rabbit polyclonal anti-D1bLIC (1:250 for IB); rabbit polyclonal anti-FLA10 (1:1000 for IB), rabbit polyclonal anti-FLA8 (1:100 for IF and 1:2000 for IB; Liang and Pan, 2013); and rabbit polyclonal anti-CNK4 (1:2000 for IB).

IFT antibodies were kindly provided by Dennis Diener and Joel Rosenbaum (Yale University, New Haven, CT). Polyclonal D1bLIC antibody was made in rabbit using the 55- to 427–amino acid protein fragment (YingJi, Shanghai, China). Rabbit polyclonal anti-CNK4 antibody was made with the two peptides RPKTPQGDMNAPPEVAGC (amino acids 297–313) and CLAQQMEELAVDDGEDED (amino acids 383–399) and affinity purified (MBL, Beijing, China).

SDS–PAGE and immunoblotting

SDS–PAGE and immunoblotting analysis were essentially as described previously (Meng *et al.*, 2014).

IF and electron microscopy

A previously published protocol was followed (Hu *et al.*, 2015). The secondary antibodies used were Texas red–conjugated goat anti-mouse immunoglobulin G (IgG; 1:400) and Alexa Fluor 488–conjugated goat anti-rabbit IgG (1:400; Molecular Probes). The samples were viewed on a Zeiss LSM780 META Observer Z1 Confocal Laser Microscope. Images were acquired and processed by ZEN 2009 Light Edition (Zeiss) and Photoshop (Adobe). Analysis for electron microscopy followed published methods (Craige *et al.*, 2010; Meng *et al.*, 2014).

Live-cell imaging

To image flagellar bulge formation and flagellar curling, DIC images were captured at 1 frame per 30 s with a Zeiss microscope (Zeiss Axio) equipped with a charge-coupled device (CCD) camera (QuantEM 512SC; Photometrics) using a 100× objective. Images were exported and processed using Photoshop and ImageJ (National Institutes of Health, Bethesda, MD).

For TIRF microscopy, cells were immobilized on coverglasses with polylysine. Images were acquired at room temperature on a Nikon microscope (A1RSi) equipped with a 100×/numerical aperture 1.49 TIRF objective and a cooled electron-multiplying CCD camera. Images were analyzed with NIS-Elements software. Kymographs and videos were generated using ImageJ, and the IFT speed and frequency were calculated.

ACKNOWLEDGMENTS

We thank Joel Rosenbaum, Dennis Diener, Robert Bloodgood, and Kaiyao Huang for provision of antibodies and strains and Wallace Marshall and Susan Dutcher for discussion during the course of this work. This work was supported by the National Basic Research Program of China (973 Program; 2012CB945003, 2013CB910700) and the National Natural Science Foundation of China (31330044; to J.P.).

REFERENCES

Badano JL, Teslovich TM, Katsanis N (2005). The centrosome in human genetic disease. Nat Rev Genet 6, 194–205.

Berman SA, Wilson NF, Haas NA, Lefebvre PA (2003). A novel MAP kinase regulates flagellar length in Chlamydomonas. Curr Biol 13, 1145–1149.

Berthold P, Schmitt R, Mages W (2002). An engineered Streptomyces hygroscopicus aph 7″ gene mediates dominant resistance against hygromycin B in Chlamydomonas reinhardtii. Protist 153, 401–412.

Bloodgood RA, Salomonsky NL (1994). The transmembrane signaling pathway involved in directed movements of Chlamydomonas flagellar membrane glycoproteins involves the dephosphorylation of a 60-kD phosphoprotein that binds to the major flagellar membrane glycoprotein. J Cell Biol 127, 803–811.

Bradley BA, Quarmby LM (2005). A NIMA-related kinase, Cnk2p, regulates both flagellar length and cell size in Chlamydomonas. J Cell Sci 118, 3317–3326.

Brazelton WJ, Amundsen CD, Silflow CD, Lefebvre PA (2001). The bld1 mutation identifies the Chlamydomonas osm-6 homolog as a gene required for flagellar assembly. Curr Biol 11, 1591–1594.

Brown J, Witman GB (2014). Cilia and diseases. Bioscience 64, 1126–1137.

Burghoorn J, Dekkers MP, Rademakers S, de Jong T, Willemsen R, Jansen G (2007). Mutation of the MAP kinase DYF-5 affects docking and undocking of kinesin-2 motors and reduces their speed in the cilia of Caenorhabditis elegans. Proc Natl Acad Sci USA 104, 7157–7162.

Cao M, Li G, Pan J (2009). Regulation of cilia assembly, disassembly, and length by protein phosphorylation. Methods Cell Biol 94, 333–346.

Cao M, Meng D, Wang L, Bei S, Snell WJ, Pan J (2013). Activation loop phosphorylation of a protein kinase is a molecular marker of organelle size that dynamically reports flagellar length. Proc Natl Acad Sci USA 110, 12337–12342.

Chan YH, Marshall WF (2012). How cells know the size of their organelles. Science 337, 1186–1189.

Chaya T, Omori Y, Kuwahara R, Furukawa T (2014). ICK is essential for cell type-specific ciliogenesis and the regulation of ciliary transport. EMBO J 33, 1227–1242.

Coene KL, Mans DA, Boldt K, Gloeckner CJ, van Reeuwijk J, Bolat E, Roosing S, Letteboer SJ, Peters TA, Cremers FP, *et al.* (2011). The ciliopathy-associated protein homologs RPGRIP1 and RPGRIP1L are linked to cilium integrity through interaction with Nek4 serine/threonine kinase. Hum Mol Genet 20, 3592–3605.

Cole DG, Diener DR, Himelblau AL, Beech PL, Fuster JC, Rosenbaum JL (1998). Chlamydomonas kinesin-II-dependent intraflagellar transport (IFT): IFT particles contain proteins required for ciliary assembly in Caenorhabditis elegans sensory neurons. J Cell Biol 141, 993–1008.

Craige B, Tsao CC, Diener DR, Hou Y, Lechtreck KF, Rosenbaum JL, Witman GB (2010). CEP290 tethers flagellar transition zone microtubules to the membrane and regulates flagellar protein content. J Cell Biol 190, 927–940.

Cross FR, Umen JG (2015). The Chlamydomonas cell cycle. Plant J 82, 370–392.

Dentler W (2005). Intraflagellar transport (IFT) during assembly and disassembly of Chlamydomonas flagella. J Cell Biol 170, 649–659.

Engel BD, Ludington WB, Marshall WF (2009). Intraflagellar transport particle size scales inversely with flagellar length: revisiting the balance-point length control model. J Cell Biol 187, 81–89.

Finst RJ, Kim PJ, Quarmby LM (1998). Genetics of the deflagellation pathway in Chlamydomonas. Genetics 149, 927–936.

Fry AM, O'Regan L, Sabir SR, Bayliss R (2012). Cell cycle regulation by the NEK family of protein kinases. J Cell Sci 125, 4423–4433.

Gaertig J, Wloga D (2008). Ciliary tubulin and its post-translational modifications. Curr Top Dev Biol 85, 83–113.

Galvan A, Gonzalez-Ballester D, Fernandez E (2007). Insertional mutagenesis as a tool to study genes/functions in Chlamydomonas. Adv Exp Med Biol 616, 77–89.

Gonzalez-Ballester D, de Montaigu A, Galvan A, Fernandez E (2005). Restriction enzyme site-directed amplification PCR: a tool to identify regions flanking a marker DNA. Anal Biochem 340, 330–335.

Hilton LK, Gunawardane K, Kim JW, Schwarz MC, Quarmby LM (2013). The kinases LF4 and CNK2 control ciliary length by feedback regulation of assembly and disassembly rates. Curr Biol 23, 2208–2214.

Hou Y, Qin H, Follit JA, Pazour GJ, Rosenbaum JL, Witman GB (2007). Functional analysis of an individual IFT protein: IFT46 is required for transport of outer dynein arms into flagella. J Cell Biol 176, 653–665.

Hu Z, Liang Y, He W, Pan J (2015). Cilia disassembly with two distinct phases of regulation. Cell Rep 10, 1803–1810.

Iomini C, Li L, Esparza JM, Dutcher SK (2009). Retrograde intraflagellar transport mutants identify complex A proteins with multiple genetic interactions in Chlamydomonas reinhardtii. Genetics 183, 885–896.

Ishikawa H, Marshall WF (2011). Ciliogenesis: building the cell's antenna. Nat Rev Mol Cell Biol 12, 222–234.

Jinkerson RE, Jonikas MC (2015). Molecular techniques to interrogate and edit the Chlamydomonas nuclear genome. Plant J 82, 393–412.
Kim S, Lee K, Choi JH, Ringstad N, Dynlacht BD (2015). Nek2 activation of Kif24 ensures cilium disassembly during the cell cycle. Nat Commun 6, 8087.
Konno A, Setou M, Ikegami K (2012). Ciliary and flagellar structure and function–their regulations by posttranslational modifications of axonemal tubulin. Int Rev Cell Mol Biol 294, 133–170.
Kozminski KG, Beech PL, Rosenbaum JL (1995). The Chlamydomonas kinesin-like protein FLA10 is involved in motility associated with the flagellar membrane. J Cell Biol 131, 1517–1527.
Kubo T, Hirono M, Aikawa T, Kamiya R, Witman GB (2015). Reduced tubulin polyglutamylation suppresses flagellar shortness in Chlamydomonas. Mol Biol Cell 26, 2810–2822.
Kubo T, Kaida S, Abe J, Saito T, Fukuzawa H, Matsuda Y (2009). The Chlamydomonas hatching enzyme, sporangin, is expressed in specific phases of the cell cycle and is localized to the flagella of daughter cells within the sporangial cell wall. Plant Cell Physiol 50, 572–583.
Lechtreck KF, Luro S, Awata J, Witman GB (2009). HA-tagging of putative flagellar proteins in Chlamydomonas reinhardtii identifies a novel protein of intraflagellar transport complex B. Cell Motil Cytoskeleton 66, 469–482.
Lefebvre PA (2009). Flagellar length control. In: The Chlamydomonas Sourcebook: Cell Motilty and Behavior, ed. GB Witman, Oxford, UK: Elsevier, 115–129.
Liang Y, Pan J (2013). Regulation of flagellar biogenesis by a calcium dependent protein kinase in Chlamydomonas reinhardtii. PLoS One 8, e69902.
Liang Y, Pang Y, Wu Q, Hu Z, Han X, Xu Y, Deng H, Pan J (2014). FLA8/KIF3B phosphorylation regulates kinesin-II interaction with IFT-B to control IFT entry and turnaround. Dev Cell 30, 585–597.
Lin H, Zhang Z, Guo S, Chen F, Kessler JM, Wang YM, Dutcher SK (2015). A NIMA-related kinase suppresses the flagellar instability associated with the loss of multiple axonemal structures. PLoS Genet 11, e1005508.
Ludington WB, Wemmer KA, Lechtreck KF, Witman GB, Marshall WF (2013). Avalanche-like behavior in ciliary import. Proc Natl Acad Sci USA 110, 3925–3930.
Luo M, Cao M, Kan Y, Li G, Snell W, Pan J (2011). The phosphorylation state of an aurora-like kinase marks the length of growing flagella in Chlamydomonas. Curr Biol 21, 586–591.
Lux FG 3rd, Dutcher SK (1991). Genetic interactions at the FLA10 locus: suppressors and synthetic phenotypes that affect the cell cycle and flagellar function in Chlamydomonas reinhardtii. Genetics 128, 549–561.
Mahjoub MR, Qasim Rasi M, Quarmby LM (2004). A NIMA-related kinase, Fa2p, localizes to a novel site in the proximal cilia of Chlamydomonas and mouse kidney cells. Mol Biol Cell 15, 5172–5186.
Mahjoub MR, Trapp ML, Quarmby LM (2005). NIMA-related kinases defective in murine models of polycystic kidney diseases localize to primary cilia and centrosomes. J Am Soc Nephrol 16, 3485–3489.
Manning DK, Sergeev M, van Heesbeen RG, Wong MD, Oh JH, Liu Y, Henkelman RM, Drummond I, Shah JV, Beier DR (2013). Loss of the ciliary kinase Nek8 causes left-right asymmetry defects. J Am Soc Nephrol 24, 100–112.
Marshall WF, Rosenbaum JL (2001). Intraflagellar transport balances continuous turnover of outer doublet microtubules: implications for flagellar length control. J Cell Biol 155, 405–414.
Meirelles GV, Perez AM, de Souza EE, Basei FL, Papa PF, Melo Hanchuk TD, Cardoso VB, Kobarg J (2014). "Stop Ne(c)king around": how interactomics contributes to functionally characterize Nek family kinases. World J Biol Chem 5, 141–160.
Meng D, Cao M, Oda T, Pan J (2014). The conserved ciliary protein Bug22 controls planar beating of Chlamydomonas flagella. J Cell Sci 127, 281–287.
Moon H, Song J, Shin JO, Lee H, Kim HK, Eggenschwiller JT, Bok J, Ko HW (2014). Intestinal cell kinase, a protein associated with endocrine-cerebro-osteodysplasia syndrome, is a key regulator of cilia length and Hedgehog signaling. Proc Natl Acad Sci USA 111, 8541–8546.
Niwa S, Nakajima K, Miki H, Minato Y, Wang D, Hirokawa N (2012). KIF19A is a microtubule-depolymerizing kinesin for ciliary length control. Dev Cell 23, 1167–1175.
O'Connell MJ, Krien MJ, Hunter T (2003). Never say never. The NIMA-related protein kinases in mitotic control. Trends Cell Biol 13, 221–228.
Omori Y, Chaya T, Katoh K, Kajimura N, Sato S, Muraoka K, Ueno S, Koyasu T, Kondo M, Furukawa T (2010). Negative regulation of ciliary length by ciliary male germ cell-associated kinase (Mak) is required for retinal photoreceptor survival. Proc Natl Acad Sci USA 107, 22671–22676.
Parker JD, Bradley BA, Mooers AO, Quarmby LM (2007). Phylogenetic analysis of the Neks reveals early diversification of ciliary-cell cycle kinases. PLoS One 2, e1076.
Pazour GJ, Dickert BL, Vucica Y, Seeley ES, Rosenbaum JL, Witman GB, Cole DG (2000). Chlamydomonas IFT88 and its mouse homologue, polycystic kidney disease gene tg737, are required for assembly of cilia and flagella. J Cell Biol 151, 709–718.
Pedersen LB, Rosenbaum JL (2008). Intraflagellar transport (IFT) role in ciliary assembly, resorption and signalling. Curr Top Dev Biol 85, 23–61.
Pigino G, Geimer S, Lanzavecchia S, Paccagnini E, Cantele F, Diener DR, Rosenbaum JL, Lupetti P (2009). Electron-tomographic analysis of intraflagellar transport particle trains in situ. J Cell Biol 187, 135–148.
Piperno G, Siuda E, Henderson S, Segil M, Vaananen H, Sassaroli M (1998). Distinct mutants of retrograde intraflagellar transport (IFT) share similar morphological and molecular defects. J Cell Biol 143, 1591–1601.
Pradel LC, Bonhivers M, Landrein N, Robinson DR (2006). NIMA-related kinase TbNRKC is involved in basal body separation in Trypanosoma brucei. J Cell Sci 119, 1852–1863.
Rosenbaum J (2003). Organelle size regulation: length matters. Curr Biol 13, R506–507.
Rosenbaum JL, Moulder JE, Ringo DL (1969). Flagellar elongation and shortening in Chlamydomonas. The use of cycloheximide and colchicine to study the synthesis and assembly of flagellar proteins. J Cell Biol 41, 600–619.
Rosenbaum JL, Witman GB (2002). Intraflagellar transport. Nat Rev Mol Cell Biol 3, 813–825.
Schneider MJ, Ulland M, Sloboda RD (2008). A protein methylation pathway in Chlamydomonas flagella is active during flagellar resorption. Mol Biol Cell 19, 4319–4327.
Scholey JM (2003). Intraflagellar transport. Annu Rev Cell Dev Biol 19, 423–443.
Shalom O, Shalva N, Altschuler Y, Motro B (2008). The mammalian Nek1 kinase is involved in primary cilium formation. FEBS Lett 582, 1465–1470.
Sirajuddin M, Rice LM, Vale RD (2014). Regulation of microtubule motors by tubulin isotypes and post-translational modifications. Nat Cell Biol 16, 335–344.
Sizova I, Fuhrmann M, Hegemann P (2001). A Streptomyces rimosus aphVIII gene coding for a new type phosphotransferase provides stable antibiotic resistance to Chlamydomonas reinhardtii. Gene 277, 221–229.
Smith LA, Bukanov NO, Husson H, Russo RJ, Barry TC, Taylor AL, Beier DR, Ibraghimov-Beskrovnaya O (2006). Development of polycystic kidney disease in juvenile cystic kidney mice: insights into pathogenesis, ciliary abnormalities, and common features with human disease. J Am Soc Nephrol 17, 2821–2831.
Sohara E, Luo Y, Zhang J, Manning DK, Beier DR, Zhou J (2008). Nek8 regulates the expression and localization of polycystin-1 and polycystin-2. J Am Soc Nephrol 19, 469–476.
Spalluto C, Wilson DI, Hearn T (2012). Nek2 localises to the distal portion of the mother centriole/basal body and is required for timely cilium disassembly at the G2/M transition. Eur J Cell Biol 91, 675–686.
Tam LW, Ranum PT, Lefebvre PA (2013). CDKL5 regulates flagellar length and localizes to the base of the flagella in chlamydomonas. Mol Biol Cell 24, 588–600.
Tam LW, Wilson NF, Lefebvre PA (2007). A CDK-related kinase regulates the length and assembly of flagella in Chlamydomonas. J Cell Biol 176, 819–829.
Thiel C, Kessler K, Giessl A, Dimmler A, Shalev SA, von der Haar S, Zenker M, Zahnleiter D, Stoss H, Beinder E, *et al.* (2011). NEK1 mutations cause short-rib polydactyly syndrome type majewski. Am J Hum Genet 88, 106–114.
Walther Z, Vashishtha M, Hall JL (1994). The Chlamydomonas FLA10 gene encodes a novel kinesin-homologous protein. J Cell Biol 126, 175–188.
Wang L, Piao T, Cao M, Qin T, Huang L, Deng H, Mao T, Pan J (2013). Flagellar regeneration requires cytoplasmic microtubule depolymerization and kinesin-13. J Cell Sci 126, 1531–1540.
Wang W, Wu T, Kirschner MW (2014). The master cell cycle regulator APC-Cdc20 regulates ciliary length and disassembly of the primary cilium. Elife 3, e03083.
Wilson NF, Lefebvre PA (2004). Regulation of flagellar assembly by glycogen synthase kinase 3 in Chlamydomonas reinhardtii. Eukaryot Cell 3, 1307–1319.
Witman GB (1992). Axonemal dyneins. Curr Opin Cell Biol 4, 74–79.
Wloga D, Camba A, Rogowski K, Manning G, Jerka-Dziadosz M, Gaertig J (2006). Members of the NIMA-related kinase family promote disassembly of cilia by multiple mechanisms. Mol Biol Cell 17, 2799–2810.
Wood CR, Huang K, Diener DR, Rosenbaum JL (2013). The cilium secretes bioactive ectosomes. Curr Biol 23, 906–911.
Yang Y, Roine N, Makela TP (2013). CCRK depletion inhibits glioblastoma cell proliferation in a cilium-dependent manner. EMBO Rep 14, 741–747.